ELSEVIER

Tectonophysics 356 (2002) 171–180

TECTONOPHYSICS

www.elsevier.com/locate/tecto

The use of uniaxial recordings in moment tensor inversions for induced seismic sources

Cezar I. Trifu*, Vladimir Shumila

Engineering Seismology Group Canada Inc., 1 Hyperion Court, Kingston, Ontario, Canada K7K 7G3

Received 20 December 2001; accepted 25 March 2002

Abstract

This study shows that the use of uniaxial recordings maintains the linear dependence of the low frequency displacements, with first polarities included, on the moment tensor components, and thus can be easily incorporated in the evaluation of failure mechanism using a moment tensor approach. Synthetic data analysis demonstrates that the errors in the orientation of the principal strain axes of the mechanism solution can be reliably evaluated using a linear error propagation approximation for up to 30% variance in the amplitude data. Case studies at the Kidd Mine indicate that the general characteristics of the mechanism solution are well retrieved, regardless of the type of data used, as relatively small disorientation angles of 15–20° are found between the solutions derived from rotated triaxial data and those from unrotated triaxial data used as uniaxial data, and of 25–30° between the solutions based on rotated triaxial data and those on independent uniaxial data.

Keywords: Uniaxial recordings; Moment tensor inversions; Seismic sources; Mine seismicity

1. Introduction

The evaluation of failure components in applications based on the monitoring of induced seismicity provides additional information on the stability of the rock mass. In the mining environment, for example, the presence of faults and joints, along with that of drifts and stopes, creates conditions for the occurrence of both shear and nonshear failures. As such, the use of the seismic moment tensor approach appears essential for the characterization of the underlying rupture mechanism. The monitoring of mine seismicity has become standard nowadays. Microseismic arrays are installed within and around the monitoring volume, and dedicated algorithms are implemented for the rapid evaluation of event locations and source parameters (Urbancic and Trifu, 2000).

In a recent paper, Trifu et al. (2000) have introduced a fast evaluation of failure components by using the far-field, point source moment tensor inversion of the spectral levels calculated in the time domain with first polarities included. Corroborating the results derived for an application at Kidd Mine (Ontario) with on-site information, Trifu and Shumila (2002) proved the reliability of these solutions. Note that their technique requires the identification of the P-, SV-, and/or SH-waves and is therefore limited to the use of three-component (triaxial) sensors. The use of uniaxial sensors, however, provides a cost-effective monitoring solution through a denser coverage of the

* Corresponding author. Tel.: +1-613-548-8287; fax: +1-613-548-8917.

E-mail address: trifu@esg.ca (C.I. Trifu).

0040-1951/02/$ - see front matter © 2002 Elsevier Science B.V. All rights reserved.
PII: S0040-1951(02)00383-9

study volume, which offers an increased event location accuracy and higher sensitivity for the same number of channels. As such, since numerous mine arrays contain mainly uniaxial sensors, it is critical to include this type of recordings in the event mechanism evaluation.

The goal of the present study is to incorporate uniaxial recordings into the moment tensor technique developed earlier and to analyze the reliability and limitations of associated inversions. Advantage is taken of the recordings provided by the Kidd Mine (Ontario) underground array that combines 23 uniaxial and 10 triaxial accelerometers. This allows for a direct comparison of results based on rotated and unrotated waveforms, as well as uniaxial and triaxial recordings, respectively. The array configuration at Kidd will be used in both synthetic and real data inversions.

2. Method

A second rank moment tensor (M_{jk}) is employed to describe, to a first approximation, a general seismic point source as seen from the far field:

$$\bar{u}_i(\mathbf{r},t) = [G_{i,jk} * \dot{M}_{jk}(t)] \tag{1}$$

where i indicates – for simplicity – both a specific location and wave type (P, SV, SH). For a homogeneous and isotropic medium, and a step time function for all moment tensor components, the expected spectral displacement field is:

$$\bar{u}_i = \sum_{k=1}^{6} c f_k^i m_k \tag{2}$$

where $c = 1/(4\pi\rho v^3 R)$, with ρ the density of the medium, v the wave velocity, R the source to sensor distance, m_k are the components of the moment tensor, and $f_k^{\mathrm{P}}, f_k^{\mathrm{SV}}, f_k^{\mathrm{SH}}$ those of the corresponding excitation matrices that depend on the take-off and azimuth angles, all in a vectorial notation (Strelitz, 1978; Trifu et al., 2000).

Signals recorded by a triaxial sensor can be rotated into the ray coordinate system, described by the unit vectors **l**, **n**, and **p**, and decomposed into the P-, SV-, and SH-wave trains. However, if only a uniaxial sensor is available, whose orientation can be described by a vector **w** containing the direction cosines with respect to the ray coordinate system, the projection of **w** on the displacements given by Eq. (2) is

$$\bar{u}_j = \sum_{k=1}^{6} c \tilde{f}_k^j m_k \tag{3}$$

where j denotes either the P or S wave (as recorded by the uniaxial sensor), and the coefficients of the excitation matrix, $\tilde{f}_k$, can be defined as

$$\tilde{f}_k^{\mathrm{P}} = f_k^{\mathrm{P}} \cdot (\mathbf{l},\mathbf{w}),\ \tilde{f}_k^{\mathrm{S}} = f_k^{\mathrm{SV}} \cdot (\mathbf{n},\mathbf{w}) + f_k^{\mathrm{SH}} \cdot (\mathbf{p},\mathbf{w}) \tag{4}$$

When the differences between observed (u_i) and theoretical ($\bar{u}_i$) displacements are normally distributed (with dispersion σ_i^2), the maximum likelihood function can be defined based on the probability density distribution function (ψ) as

$$L(\bar{u}_i|\mathbf{m}) = \sum_i \log(\psi_i) = -1/2 \sum_i [(u_i - \bar{u}_i)^2/\sigma_i^2] - \sum_i \log\sigma_i^2 + \text{constant} \tag{5}$$

At the optimal point, where L is maximum, the first derivatives with respect to model parameters must be zero

$$\partial L(\mathbf{m})/\partial m_j = \sum_i [(u_i - \bar{u}_i) c f_j^i/\sigma_i^2] = 0 \tag{6}$$

After substitution (using Eqs. (2) and (3)), a linear system of equations in the moment tensor components is obtained, whose solution describes the event mechanism. Observational data are the spectral levels of the P-, SV-, and SH-wave trains from triaxial recordings, and P-and S-waves from uniaxial recordings, calculated in the time domain and with first polarities included, respectively (Trifu et al., 2000). The overall effect of adding the uniaxial recordings is an increase in the number of equations and, if the spectral levels and first wave polarities are evaluated with a similar consistency, an increase in the solution quality.

3. Array configuration

A volume of about $300 \times 300 \times 600$ m, located approximately between 1500 and 2100 m depth, is currently monitored at Kidd Mine in Timmins (Ontario) by a microseismic array consisting of 10

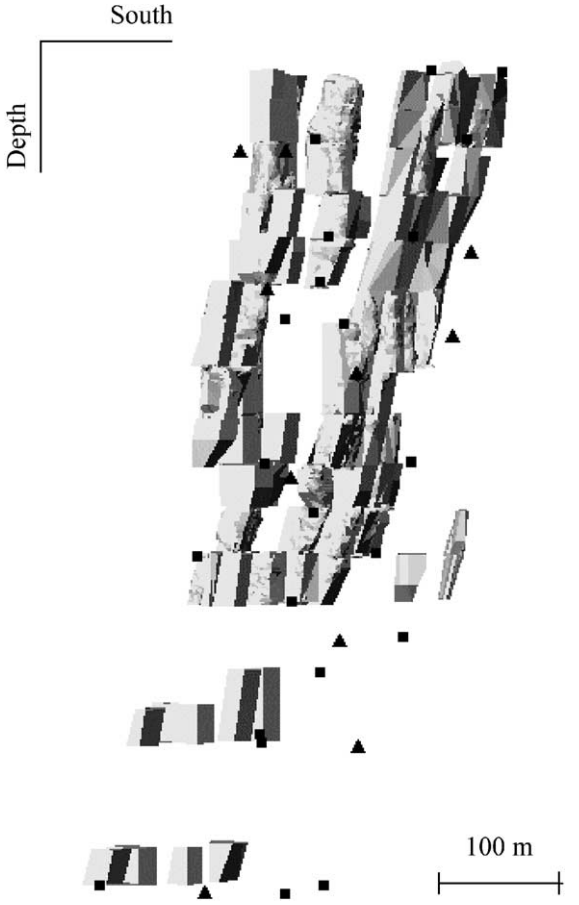

Fig. 1. View of the microseismic array at Kidd Mine in a South–Depth projection; triangles and rectangles correspond to the locations of triaxial and uniaxial accelerometers, respectively. Shaded blocks indicate backfilled areas.

triaxial and 23 uniaxial accelerometers homogeneously distributed underground (Fig. 1). The triaxial accelerometers (ESG A3003) have a flat response between 1 Hz and 5 kHz ($\pm$ 3 dB) at a sensitivity of 3 V/g, whereas the frequency bandwidth of the uniaxial accelerometers (ESG A1030) is between 50 Hz and 5 kHz ($\pm$ 3 dB) at a sensitivity of 30 V/g. The signals are digitized at 20 kHz sampling rate, multiplexed underground, and transmitted via fiber optic cables to the data acquisition system on the surface.

The sensitivity of the microseismic array allows for events as small as moment magnitude -2.5 to be located to within 10–20 m accuracy. Events with moment magnitudes between -1 and 0 usually generate unclipped recordings at five or more triaxial sensors. In order to study the accuracy of event mechanism inversions, both synthetic and real data are used. Since the purpose of this work is methodological, microseismic event locations within the monitoring volume are randomly selected for analysis (Table 1). All the case studies in this paper are based on the actual microseismic array configuration installed at Kidd.

4. Inversion quality

Since Eq. (6) remains linear in the moment tensor components, whether triaxial or uniaxial recordings are used, the information provided by uniaxial sensors can easily be incorporated in the inversion technique previously described by Trifu et al. (2000). The random errors associated with the moment tensor estimate depend on how well the model will fit the data under the existing noise level and signal measuring errors. A statistically optimal data fit provides unbiased estimates of the moment tensor components, $\hat{m}_k$, and their associated covariance matrix, e_{jk}.

The event mechanism solution is defined by the principal strain axes P, B, and T (parallel to the principal stresses in a homogeneous and isotropic medium), the relative size and orientation of which are derived from the tensor's eigenvalues $\{\lambda_i\}$ and

Table 1
List of the seismic events used in this study; Err denotes the location error in a vectorial sense and N is the number of first P- and S-wave arrivals used in the event location

Event #	Date (ddmmyy)	Time (hh:mm:ss)	North (m)	East (m)	Depth (m)	Err (m)	N
1	121000	16:38:16	65617	65786	1715	12	22
2	201000	03:06:19	65683	65562	2056	14	17
3	121100	08:04:59	65754	65616	1588	17	24
4	151100	13:09:04	65607	65759	1713	19	21
5	140101	09:43:41	65763	65817	1498	19	29

eigenvectors $\{\mathbf{v}_i\}$ ($i=1, 2, 3$), respectively. In the general case, the evaluation of the statistical distributions of eigenvalues and eigenvectors based on the known distribution of random moment tensor components represents a challenging problem, whose theoretical complexity has been outlined by Xu (1999). The solutions derived are far too complicated and cannot be applied in common practice.

Based on the assumption that the standard deviation of any parameter estimate is small and can be modeled by a normal probability distribution, a much simpler and therefore practical solution can be proposed, consisting of a linear error propagation approximation. This allows for a parameter q that depends on the moment tensor components to be defined as

$$q = \hat{q} + \sum_k \frac{\partial q}{\partial m_k} \Delta m_k \tag{7}$$

where $\hat{q}$ is the estimate and the variance is given by

$$\sigma_q^2 = \sum_j \sum_k \frac{\partial q}{\partial m_j} \frac{\partial q}{\partial m_k} e_{jk} \tag{8}$$

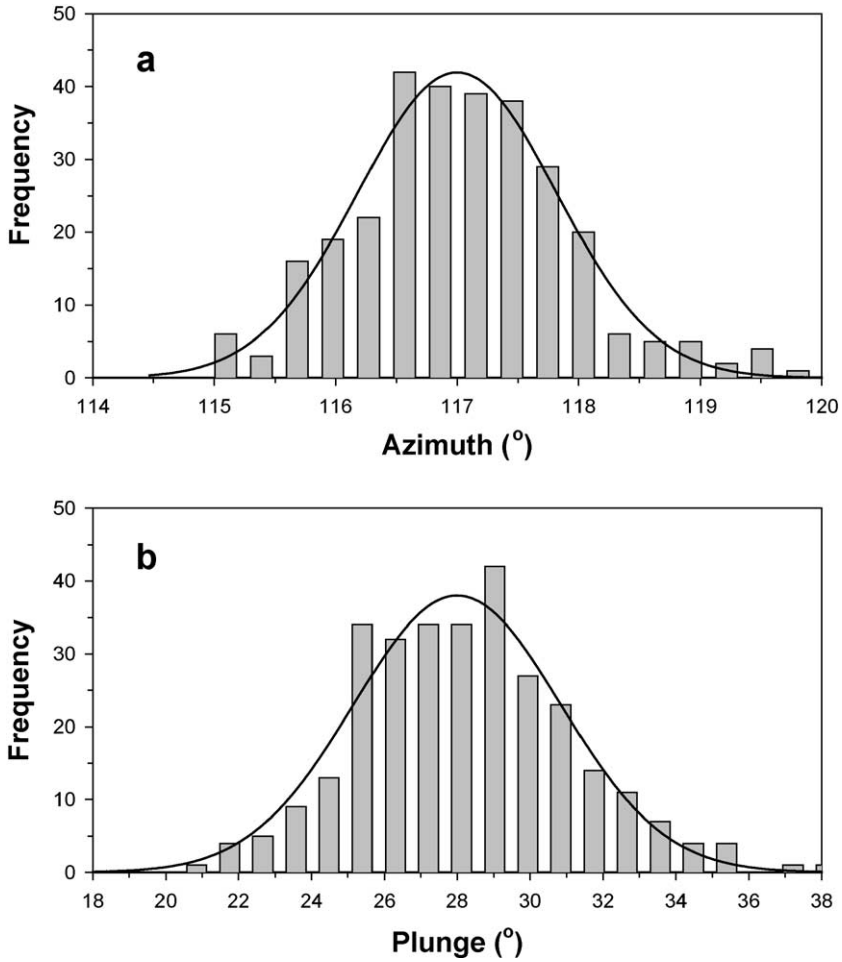

Fig. 2. Histograms of the (a) azimuth and (b) plunge angles of the P axes for 300 inversions on synthetic amplitude data sets corresponding to a specific double-couple mechanism (see text) and incorporating a variance of 10%. The normal distribution that best approximates the histograms is also shown, for reference.

Based on the definition of eigenvalues and eigenvectors, $\lambda_i=(\mathbf{v}_i, \mathbf{M}\mathbf{v}_i)$, the variance of any eigenvalue can be calculated using Eq. (8)

$$\sigma_\lambda^2 = v_1^2\sigma_{m_1}^2 + v_2^2\sigma_{m_4}^2 + v_3^2\sigma_{m_6}^2 + 2v_1v_2r_{14} + 2v_1v_3r_{16} + 2v_2v_3r_{46} \quad (9)$$

where v_1, v_2, and v_3 are the components of the corresponding eigenvector and r_{ij} is the correlation coefficient between the m_i and m_j estimates. In order to evaluate the standard deviation of the principal strain axes (i.e., of their azimuth and plunge angles), the spectral equation $\mathbf{M}\mathbf{v}_i=\lambda_i\mathbf{v}_i$ is used to eliminate λ_i, and after summing up the resulting equations, the following expression that links moment tensor components and eigenvectors is obtained

$$\begin{aligned} F(\mathbf{m},\mathbf{v}) \equiv {} & (m_1-m_4)v_1v_2 + (m_1-m_6)v_1v_3 \\ & + (m_4-m_6)v_2v_3 + m_2(v_2^2-v_1^2) \\ & + m_3(v_3^2-v_1^2) + m_5(v_3^2-v_2^2) \\ & + (m_2v_3-m_3v_2)v_1 + (m_2v_3-m_5v_1)v_2 \\ & + (m_3v_2-m_5v_1)v_3 = 0 \end{aligned} \quad (10)$$

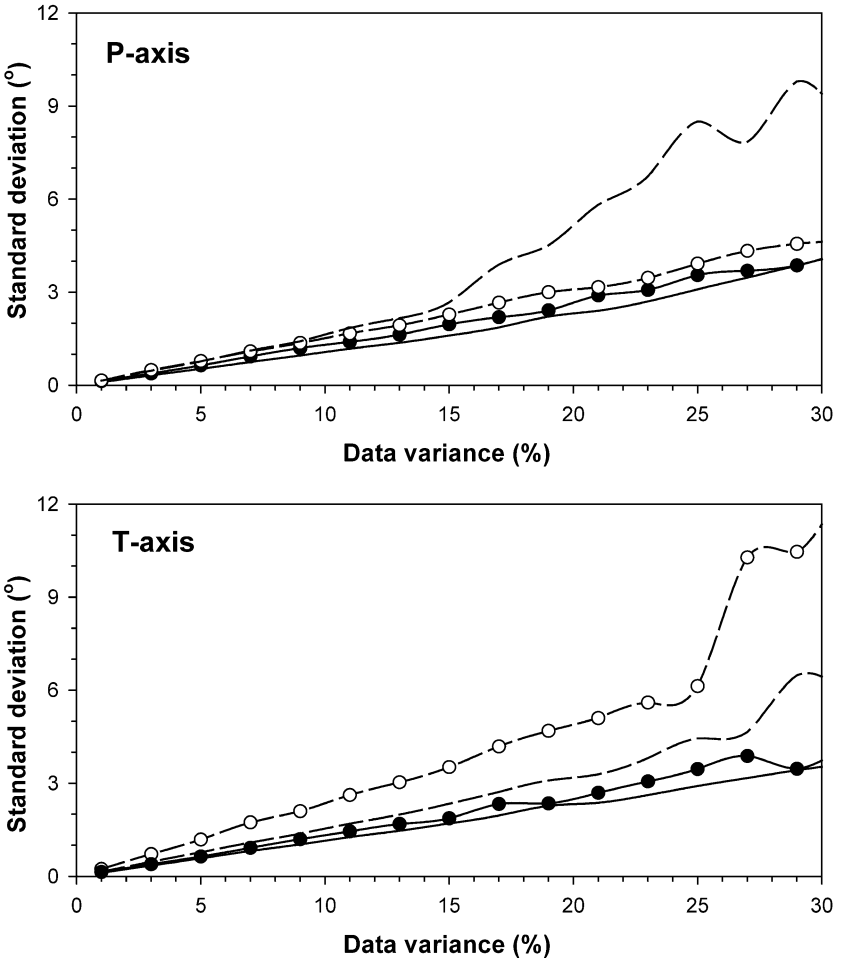

Fig. 3. Standard deviation of the azimuth (solid symbols and lines) and plunge angles (open symbols and dashed lines) as a function of data variance. The lines with symbols correspond to the results obtained from inversions on randomly altered data sets within data variance limits. The lines without symbols correspond to the standard deviations derived using a linear error propagation approximation.

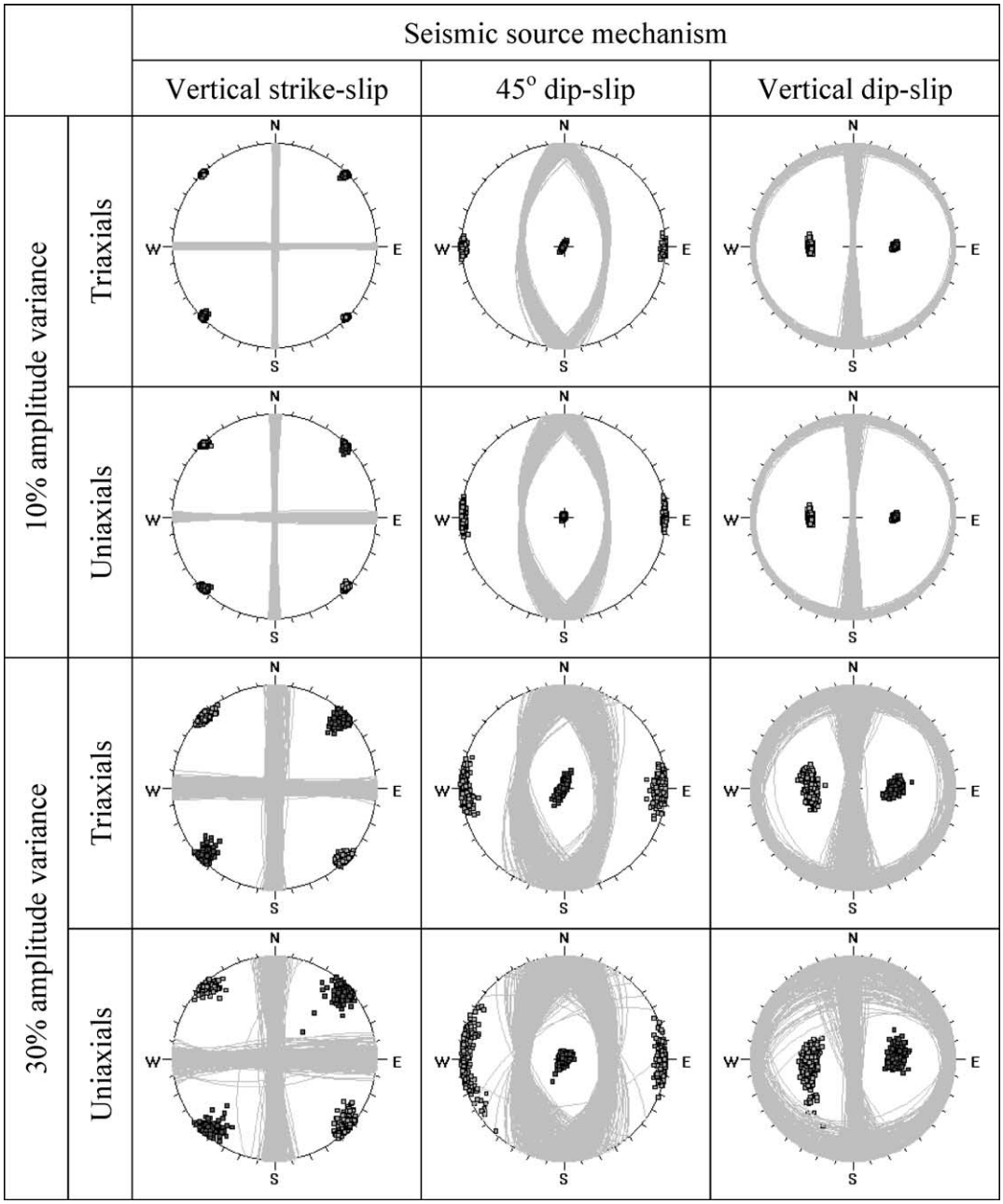

Fig. 4. Comparison of source mechanism inversions from synthetic rotated triaxial data and the first component of unrotated triaxial data treated as uniaxial data, respectively. Three basic double-couple mechanisms were employed to randomly generate 300 data sets per case within specific amplitude variance limits. A lower hemisphere projection is used, on which open and solid symbols denote the P and T axes, respectively.

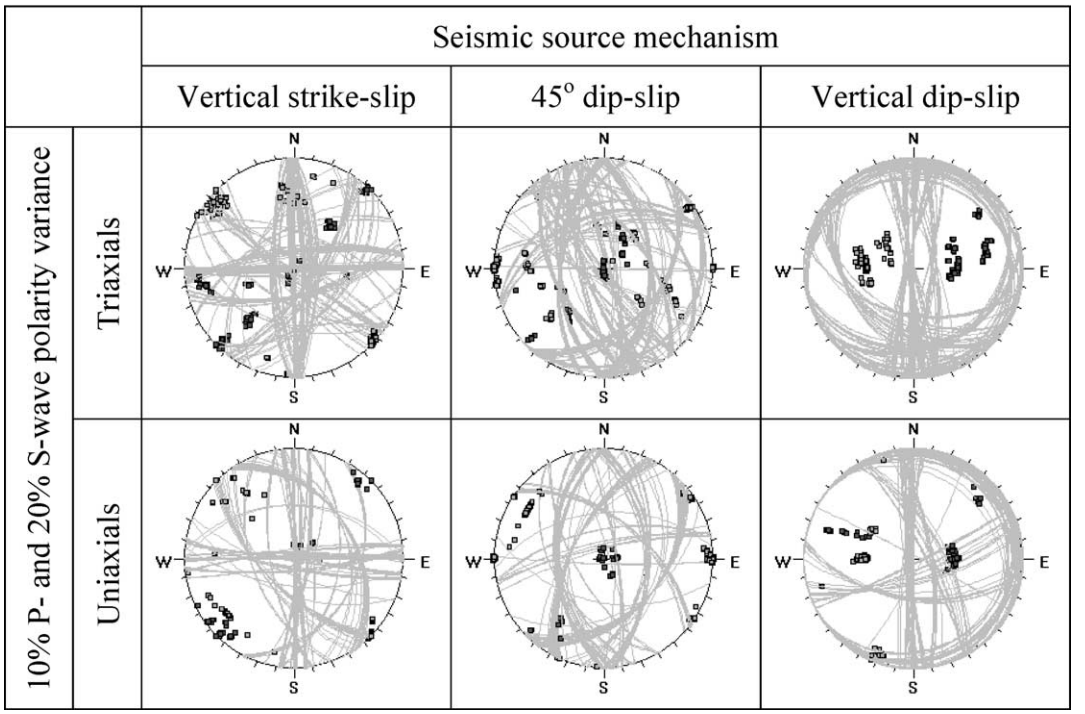

Fig. 5. Comparison of source mechanism inversions (see also Fig. 4) from synthetic data altered within specific polarity limits for three basic double-couple mechanisms.

The eigenvector components can be written as

$$\mathbf{v} \equiv [\sin(\delta)\cos(\varphi),\ \sin(\delta)\sin(\varphi),\ \cos(\delta)] \qquad (11)$$

where φ and δ are the parameters of interest, the azimuth and plunge angles, respectively. These parameters can be evaluated based on Eq. (7), where the derivatives are calculated as follows

$$\frac{\partial \delta}{\partial m_k} = -\left(\frac{\partial F}{\partial m_k}\right) \Big/ \left(\frac{\partial F}{\partial \delta}\right),$$

$$\frac{\partial \varphi}{\partial m_k} = -\left(\frac{\partial F}{\partial m_k}\right) \Big/ \left(\frac{\partial F}{\partial \varphi}\right) \qquad (12)$$

5. Case studies on synthetic and real data

In order to test the performance of the above error evaluation procedure, the following synthetic case study was used. For an arbitrary double-couple source mechanism ($P_{az}=117°$, $P_{pl}=28°$, $T_{az}=12°$, $T_{pl}=26°$), a full set of spectral amplitudes was generated, with first polarities attached, for Event #1 (Table 1) as recorded by the 10 triaxial sensors currently installed at Kidd Mine, Ontario (Fig. 1). Noise was modeled in amplitude as a Gaussian distribution with predefined variance. For each value of the variance, a total of 300 data sets were randomly generated and then inverted to retrieve the mechanism solutions (Fig. 2). Fig. 3 presents the

Table 2
The size of the data set employed in event mechanism determination from rotated triaxial waveforms (T), unrotated triaxial waveforms treated as uniaxial waveforms (TU), and uniaxial waveforms recorded at uniaxial sensor locations (U), along with the disorientation angle for solution pairs

Event #	Sample size			Disorientation angle (°)	
	T	TU	U	T–TU	T–U
1	22	21	16	16	30
2	15	14	17	17	33
3	19	19	18	14	26
4	23	24	26	18	26
5	25	25	29	11	25

Event #	Triaxials	Triaxials as Uniaxials	Uniaxials
1	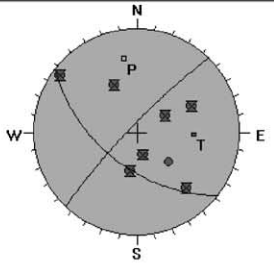	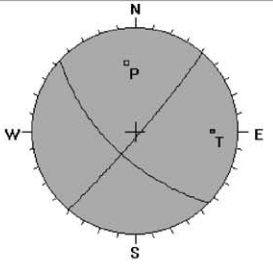	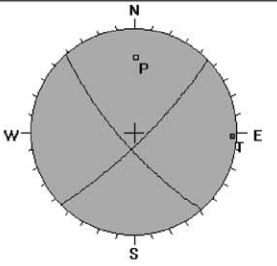
2	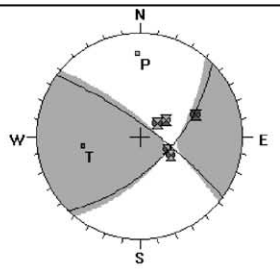	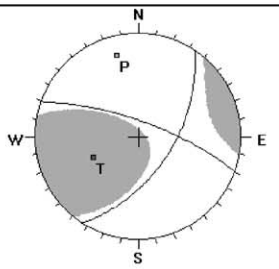	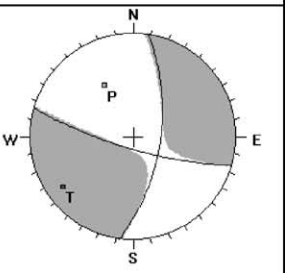
3	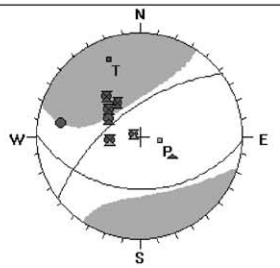	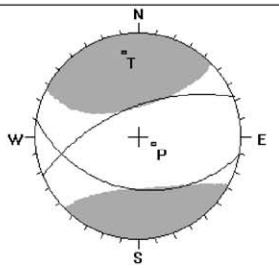	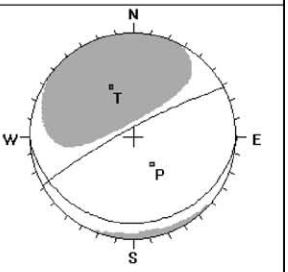
4	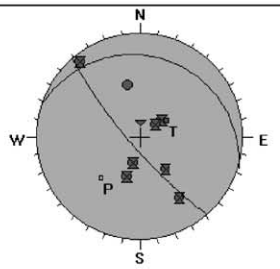	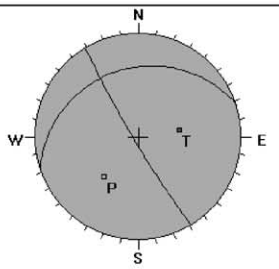	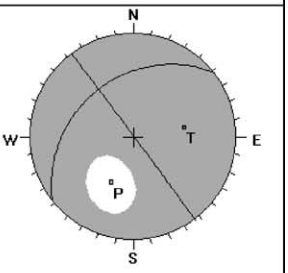
5	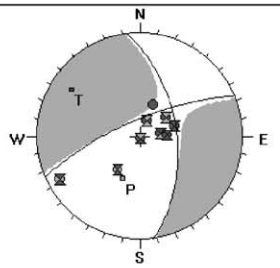	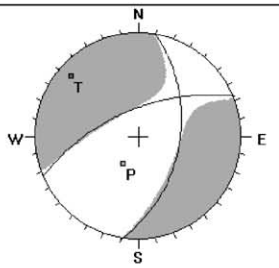	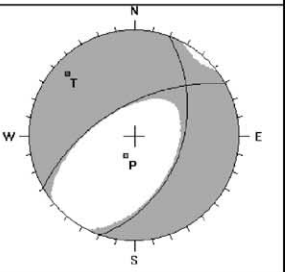

observed standard deviation of these solutions as a function of data variance. The error propagation technique was then employed to calculate predicted standard deviations. The results obtained show that although the errors are relatively small, the difference between the observed and predicted values increases with increasing variance in the data. It appears, however, that the linear error propagation provides a very good approximation, to within 1° for up to 15% variance, and 5° for up to 30% variance in the amplitude data.

The observed data contain two main sources of uncertainty: errors in spectral level estimates and first arrival polarities. Consequently, before using uniaxial recordings in moment tensor inversions on real data for event mechanism determination, several additional synthetic tests are proposed for assessing the reliability of the results derived. The first type of error is modeled as random (Gaussian) noise with a zero mean value and a standard deviation corresponding to specific values of the variance in each spectral level estimate. To simulate the first polarity errors, a predefined percentage of the polarities corresponding to each wave type data set is randomly altered. Three basic event mechanism solutions were selected, a vertical strike-slip faulting, a 45° dip-slip faulting, and a vertical dip-slip faulting (Jost and Herrmann, 1989) for a source location similar to that of Event #1. In order to better simulate a real situation, synthetic data were only generated for those phases (P, SV, SH) that were identified in the actual triaxial recordings. Subsequently, a uniaxial seismic network was defined by retaining only the first channel of each triaxial sensor. This ensures a data sample of comparable size for each of the inversions based on triaxial and uniaxial data, respectively.

The results of this test are shown in Figs. 4 and 5. Each image is a lower hemisphere projection of the event mechanism solutions derived for 300 data sets randomly selected within the specified amplitude and polarity variance. Although the use of uniaxial recordings leads to an additional 5–10° spread in the orientation of the inverted principal strain axes as compared to triaxial recordings, it can be concluded that it provides reliable inversions even for 30% amplitude variance (Fig. 4). Uncertainties in the first polarity picking, however, have a significant effect on the results derived, suggesting that the data for which polarities cannot be correctly identified should be discarded (Fig. 5).

An ideal comparison between the use of uniaxial and triaxial data in the evaluation of the source mechanism would require a data sample of the same size and spatial distribution with respect to the seismic source. In order to best approximate these conditions, unrotated triaxial recordings can be treated as those obtained from three independent uniaxial sensors. There are, however, several practical limitations to this procedure. For example, one triaxial sensor can provide a maximum of three data points, corresponding to the identified P-, SV-, and SH-waves, whereas the interpretation of the same recordings as provided by three uniaxial sensors could offer six uniaxial data, three for each of the P- and S-wave data. This has the potential to create data samples of different size, with implications on the inversion process. However, since first wave arrival and polarity cannot always be resolved from unrotated signals, the use of three uniaxial recordings at one location may actually provide less than six data points.

With the above considerations in mind, an analysis was carried out on five recorded events (Table 1) exhibiting different data coverage on the focal sphere and characterized by different mechanisms. The analysis was exclusively based on signals with clear first wave polarities. For each event, the mechanism solutions obtained for various data sets were compared to each other by calculating the disorientation angle (Table 2), which represents the minimum rotation angle necessary to make two solutions coincide (Kagan, 1991). The results, presented in Fig. 6, show that the general characteristics of the mechanism solution are well retrieved, regardless whether triaxial or uniaxial data are employed. Disorientation

Fig. 6. Comparison of source mechanism inversions for five microseismic events recorded at the Kidd Mine; inversions are based on triaxial data, triaxial data treated as uniaxial data, and independent uniaxial data, respectively. For triaxial waveform inversions, the observed P, SV, and SH data are shown on the focal sphere as circles, up-triangles and down-triangles, with open and solid symbols denoting their negative and positive polarities, respectively. The shaded areas on the focal sphere correspond to dilatational motions in the P-wave radiation for the derived solution.

angles of up to 15–20° were calculated between the solutions derived from rotated triaxial data and those from unrotated triaxial data used as uniaxial data, and up to 25–30° between the solutions based on rotated triaxial data and those on independent uniaxial data.

6. Conclusions

The monitoring of induced seismicity for engineering applications such as those encountered in mines commonly employs uniaxial sensors along with a limited number of triaxial sensors. For any given number of channels, the use of uniaxial sensors allows for a denser array configuration that ensures a higher sensitivity and increased event location accuracy. In view of the numerous uniaxial sensors currently installed in mines, this study shows that the use of uniaxial recordings maintains the linear dependence of the low frequency displacements, with first polarities included, on the moment tensor components, and can thus be easily incorporated in the evaluation of failure mechanism using a moment tensor approach.

Synthetic data analysis reveals that the errors in the azimuth and plunge angles of the mechanism solution's principal strain axes can be evaluated using a linear error propagation approximation. The differences between the observed and calculated errors are to within 1° for up to 15% variance, and 5° for up to 30% variance in the amplitude data. Additional synthetic studies carried out on case study mechanisms (vertical strike-slip, 45° dip-slip, and vertical dip-slip faulting) indicate that uniaxial data lead in average to similar results as triaxial data under the presence of random noise equivalent to 30% amplitude variance, but with a 10° increase in the dispersion of azimuth and plunge angles of strain axes. The inversions though are drastically influenced by errors in first polarities, suggesting that the data for which the polarity information cannot be clearly identified should be discarded.

Real data analysis at the Kidd Mine concludes that the general characteristics of the mechanism solution are well retrieved, regardless whether triaxial or uniaxial data are employed. This is supported by the relatively small disorientation angles of 15–20° calculated between the solutions derived from rotated triaxial data and those from unrotated triaxial data used as uniaxial data, and of 25–30° between the solutions based on rotated triaxial data and those on independent uniaxial data. Providing that the data evaluation process is carried out with the same consistency regardless of the type of recordings used, the incorporation of the uniaxial data in moment tensor inversion will ensure an increased solution quality.

Acknowledgements

We would like to thank Kidd Mining Division, Falconbridge Ltd. for the permission to use their data and Norm Disley for providing us with an updated visualization of the mining operations. We express our thanks to Diane Doser for her comments and suggestions on the manuscripts.

References

Jost, M.L., Herrmann, R.B., 1989. A student's guide to and review of moment tensors. Seismol. Res. Lett. 60, 37–57.

Kagan, Y.Y., 1991. 3-D rotation of double-couple earthquake source. Geophys. J. Int. 106, 709–716.

Strelitz, R.A., 1978. Moment tensor inversions and source models. Geophys. J. R. Astron. Soc. 52, 359–364.

Trifu, C.-I., Shumila, V., 2002. Reliability of seismic moment tensor inversions for induced microseismicity at Kidd Mine, Ontario. Pure Appl. Geophys. 159, 145–164.

Trifu, C.-I., Angus, D., Shumila, V., 2000. A fast evaluation of the seismic moment tensor for induced seismicity. Bull. Seismol. Soc. Am. 90, 1521–1527.

Urbancic, T.I., Trifu, C.-I., 2000. Recent advances in seismic monitoring technology at Canadian mines. J. Appl. Geophys. 45, 225–237.

Xu, P.L., 1999. Spectral theory of constrained second-rank symmetric random tensors. Geophys. J. Int. 138, 1–24.